Interdisciplinary Approach for the 3D Analysis of Spinal Growth Modulation as a *Novel* Fusionless Scoliosis Treatment

Diana Glaser, PhD[1,2]
Josh Doan, MEng[1]
Vidyadhar Upasani[3]
Christine Farnsworth, BS[2]
Peter Newton, MD[2]

[1] Orthopedics Biomechanics Research Center, San Diego, CA
[2] Department of Orthopedics, Rady Children's Hospital, San Diego, CA
[3] University of California, San Diego, CA

Address Correspondence to:
Diana Glaser, PhD
3020 Children's Way, MC 5054
San Diego, CA 92123

Phone: 858-966-1700 x 4857
Fax: 858-966-7494
DGlaser@rchsd.org

Running Title: 3D Analysis of Novel Scoliosis Treatment

Study Design: In Vivo Animal Study

Objective: To develop and evaluate a new interdisciplinary approach for the 3D analysis of spinal growth modulation as a novel method for fusionless scoliosis treatment.

Summary: Scoliosis has for a long time been recognized as a three-dimensional (3D) deformity; still 3D morphological analyses are scarce. The third dimension is however critically important, but it presents a great challenge due to the classical two-dimensional (2D) radiographic view. This study introduced scoliosis by anterolateral spinal tethers in a mini-pig model. Classical 2D measurements off the plane X-Rays/CT were compared to 3D CT reconstructions. Our new 3D approach for advanced imaging analysis showed subtle difference between the 2D and 3D assessments.

Introduction: Most previous research concentrated on 2D geometrical analysis determined by plane X-Rays. The objective of this study was to quantify 3D spinal deformation and to compare with 2D measurements. In particularly: 1) the reproducibility of each method; 2) the inter-method correlation; and 3) advanced 3D scoliosis curve quantification were explored.

Methods: Twelve seven month old mini-pigs received anterolateral thoracic vertebral screws in four consecutive thoracic vertebrae (T8 to T11). In six of the animals screws were connected by a polyethylene tether across three adjacent motion segments, while six animals received sham only surgeries. For the 2D evaluation, X-Rays and 2D CT scans at 6mo post-operative (OP) were used to measure scoliosis and kyphosis Cobb angle, vertebral body (VB) and intervertebral disk (IVD) space wedging, anterior, posterior, left and right disc height. Using Mimics, CT images were segmented semi-automatically and 3D surfaces reconstructed. Custom MATLAB application was used to assess from the 3D reconstruction automatically the same parameters as specified in the 2D analysis. Additionally, maximal plane of deformation, maximum Cobb angle, maximum VB and IVD wedging off the 3D were documented. Further, μCT and MRI reconstructions allowed for the evaluation of growth plate and disc, respectively, which is not possible under conventional 2D techniques. 2D reproducibility was determined by performing all measurements by two independent researchers at 2 different occasions. The inter- and intra-class correlation (ICC) was determined. Linear regression determined the inter-method correlation between the 2D and 3D results. The means from each correlation were compared by repeated ANOVAs.

Results: Radiographs, 2D and 3D CT images demonstrated significant three-dimensional deformity creation in the tethered animals compared to sham controls. There was excellent correlation of 2D and 3D measurements when evaluating the coronal and sagittal Cobb angle.
Inter- and intra- class correlation was also very high for the Cobb measurements, indicating good reproducibility of the results. The correlation between 2D and 3D measurement methods is good for the most other parameters. Care has to be taken when created deformity is very large and deviation between local (vertebra) and global coordinate system increases. In such cases, 2D views don't allow for accurate capture of the 3D characteristics and lead to larger errors as seen in the evaluation of the vertebra body wedging. Disc heights measured from 3D MRI were in the sham group (1.87±0.07mm) significantly higher when compared to the tethered group (1.65±0.1mm). In particularly, the anterior right and left sectors were significantly reduced in the tethered group.

Conclusion: 3D results show subtle deviation from 2D measurements, even though there is a correlation between both methodologies. The small angles involved make 2D evaluations are very sensitive to the lines drawn by the user on the radiographic films, which resulted in large intra- and inter-observer variation, particularly when evaluating vertebra body wedging. The automated procedure, associated with the 3D analysis, allows for a more consistent selection and is not biased by the user. In addition, 2D measurements are dependent on the plane at which the image was taken. The maximal plane of deformation frequently is located outside the plane coronal or lateral view. Previous clinical and in vivo animal research concentrated on the 2D geometrical changes as determined by plane radiographs. New evaluation values were possible when extending the analysis into the 3D space. The 3D view of the system allowed for analysis of the screw placement accuracy and for identification of the maximal plane of deformation, both of which are not possible with either of the 2D methods. Our new 3D advanced imaging techniques will allow for better description of spinal deformities.

Key words: CT, microCT, scoliosis, AIS, 3D reconstructions, anterolateral flexible tether, fisionless scoliosis treatment, spinal growth modulation

SIGNIFICANCE

Scoliosis affects 2-3% of adolescents in the US. Idiopathic scoliosis (IS) is a complex structural 3D spinal deformity resulting >500,000 doctor visits per year[1] and often progresses rapidly during the adolescent growth spurt[2,3]. Many cases (1-3 per 1,000 school children) require immediate treatment with bracing or surgery[4]. Severe childhood and adolescent scoliosis can become symptomatic, leading to pain accompanied by cardiopulmonary compromise[5].

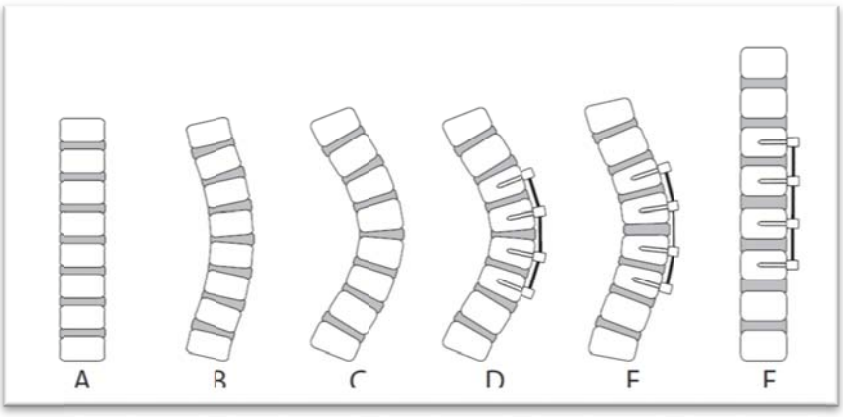

Figure 1. Progression of scoliosis with growth from a straight spine (A), with disc wedging (B), and finally vertebral wedging (C). If the deformity is treated with a tether to growth placed on the convex side (D), discs straighten (E), then finally vertebrae grow straight (F). Once the tether is removed or cut, the spine has theoretically returned to a normal straight spine.

CURRENT PROBLEMATIC

There is a lack of pediatric spinal implants designed to correct scoliosis in children without performing an associated fusion.

The current standard treatment for large progressive curves is spinal fusion which allows immediate deformity correction and prevents further deformity progression. However, this requires arthrodesis over multiple intervertebral levels in a growing spine, sacrificing further growth, motion and trunk flexibility and impacting height and pulmonary development[3]. Scoliosis management with bracing comes with patient compliance concerns and, at best, limits

progression without hope of lasting correction. An alternative treatment option that harnesses the remaining growth of the spine to permanently correct the deformity, prevent further progression, preserve spinal flexibility and allow further growth, is becoming an appealing option that would substantially improve the quality of life of those with spinal deformities. Fusionless surgical techniques have emerged that aim to correct deformities by modulating the growth of the spine (Fig. 1). Currently, the mechanism of modulating spinal growth is not well understood, which lead to the rationale of the present study. We evaluated a clinically relevant fusionless scoliosis implant on a large animal model while inducing a spinal deformity (inverse approach to correcting scoliosis) and analyzing the short-effects on each component of the spine.

Preclinical data in an immature animal model is an important step towards developing a new standard of treatment. In the present study we utilized a potential device and a strategy that is applicable to the correction of scoliosis in growing children and adolescents by modulating/redirecting the growth of the scoliotic spine. The rationale for using deformity creation to assess device efficacy is due to the lack of an animal model with naturally occurring scoliosis. Therefore, normal animal spines will have these fusionless devices implanted to modulate their spinal growth and create, rather than correct, deformity (Fig. 2). The clinical application would be the inverse analog, where a child with scoliosis would have the optimal fusionless device implanted to modulate their spinal growth and correct existing deformity (Fig. 1). Although, it is not clear that the mechanisms that create deformity in an animal model will be identical to those required to correct scoliosis in a patient, we believe the responses of the vertebral body and intervertebral disc to tethering will in fact be similar to the clinical condition. Although methods to create scoliosis in animals (goats) [38] do exist, the technique involves first tethering the spine posteriorly to create the “scoliosis”. Thus mechanisms to correct a deformity

created by posterior tethering with contralateral anterior tethering seem counter-intuitive and may not offer additional information. For these reasons we have chosen a model that studies the growth and metabolic responses to primary anterior growth tethering rather than attempting to correct an artificially created deformity.

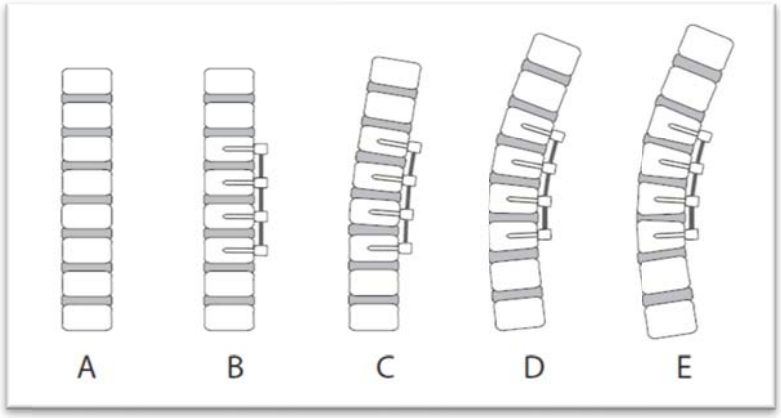

Figure 2. Experimental growth modulation starting with a straight animal spine (A). A tether to growth is placed unilaterally (B), first resulting in deformity of IVD (C), then VB wedging with straightening of the IVD (D) and finally, VB wedging to create deformity with a metabolic response of the disc which results in "reverse" wedging of the disc (E).

INNOVATION

The concept of growth modulation treatment has been well-described with respect to the management of long-bone deformities such as knock-knees and bowed legs (genu valgum and varum)[3,47,48] (Fig. 3A). This experience provides the rationale for applying growth modulation strategies to the treatment of vertebral deformities in scoliosis. The ability to modulate vertebral physes with skeletal fixation devices was initially confirmed in small animal studies demonstrating that mechanical modulation of vertebral body growth can be described according to the Hueter-Volkman Law[23,25-28]. Early clinical results of vertebral interbody stapling were disappointing[49,50] but current staple designs using Nitinol, have shown promising results in a goat

scoliosis model[38]. Recent clinical studies show feasibility of vertebral body stapling for scoliosis treatment suggesting at least stabilization of progressive scoliosis[39,40] (Fig. 3B).

A different fusionless treatment option using a flexible tether mechanism has been suggested and preliminarily investigated by Newton et al. [24,29-31]. The tether applies similar principles of mechanically harnessing and redirecting the growth of the spine as seen in the long bone staple technique (Fig. 3C). The load application through a flexible instead of rigid implant promises better initial (IVD) and ultimate (VB and IVD) correction in all planes when compared to a more rigid staple. Preserved long term disc health may be anticipated as motion, particularly torsion, is allowed while the tether is in place. Placement of vertebral body screws anterolaterally within the vertebra using minimally invasive thoracoscopic methods is well described approach for spinal fusion. Clinical application would also utilize this minimally invasive approach. Preliminary studies show very encouraging results with predictable growth modulation and deformity creation in large animal models (approximating the magnitude of idiopathic scoliosis clinically)[24,29-32]. Other research groups found the tether to provide greater shape changes and better fixation than the staples, and histological evidence of fibrous tissue around the staple tines, adding strength to our assumption of greater efficacy and integrity of the tether when compared to the rigid staple[33,35,37].

Fusionless scoliosis surgery is an emerging treatment for idiopathic scoliosis as it offers theoretical advantages over current forms of treatment. As the etiological pathway underlying scoliosis remains unclear, it requires a 3D interdisciplinary analysis incorporating a range of physiological assessments.

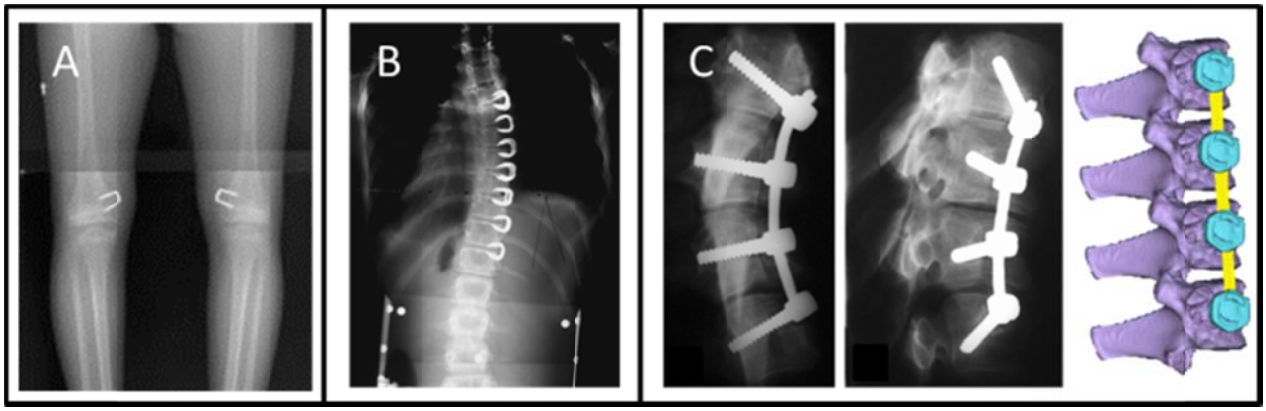

Figure 3. Staple application for long-bone deformities[51] (A); SMA staple in human spine[39] (B); Flexible tether experimental application with 3D schematic, PA and lateral views[30] (C).

RATIONALE

The multidisciplinary approach we are proposing is essential to solve the numerous open questions resulting from the underlying, still widely unclear, multifactorial etiology of idiopathic scoliosis and is associated with the complicated mechanism of spinal growth modulation. Current generally accepted pathogenesis theories include the anterior overgrowth mechanism and biomechanical pathogenesis. Growth modulation originates from the concept of anterior spinal column overgrowth causing mechanically applied compressive loading on the physes leading then to alterations in vertebral growth. [17,29]. Once initiated, further progression of scoliosis may occur based upon the Heuter-Volkman principle; that bony expansion at a growth plate is inhibited by mechanical compression and stimulated by distraction resulting in first vertebra then disc wedging which then leads to self-perpetuating deformity progression.[46] (Fig. 4, vicious cycle).

Previous research concentrated on the 2D geometrical changes as determined by plane radiographs and some histological analysis. With our current study, we applied 3D advanced imaging techniques allowing us to make an important step towards a thorough description of the mechanical spinal growth modulation and its efficacy. No previous research has tried to

thoroughly and systematically describe these 3D alterations by incorporating 3D CT for vertebra reconstruction, 3D μCT for physis and end plate evaluation and MRI for disc assessment. Volumetric analysis and spatial maps generate a novel way for the functional material property description.

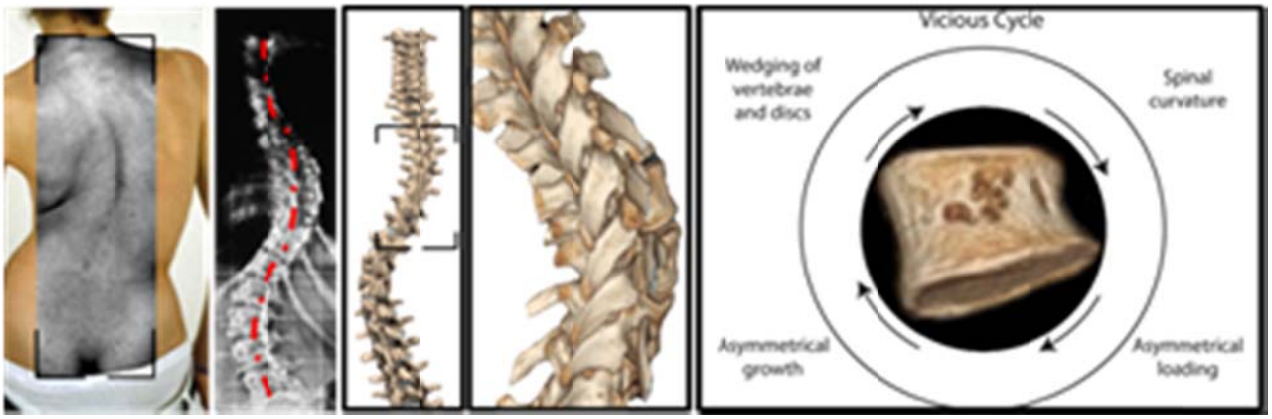

Figure 4: Idiopathic Scoliosis (from the left); 2D spinal XRay; 3D CT reconstruction; Scoliotic spine with lateral and rotatory deformation and approximation of the spinous processes; Vicious cycle of vertebral wedging.

METHODS

Animal Model

A previously reported Yucatan mini-pig model of spinal growth modulation using an anterolateral flexible tether will be utilized[24,32]. This animal was selected due to similarities between the thoracic spine of immature mini-pigs and that of the juvenile/adolescent human, including a growth rate on the order of magnitude as that during the adolescent growth spurt and similar vertebral shape (height/diameter ratio). The mini-pig thoracic spine also approximates the size of the juvenile human spine at the time of surgery (animals aged 6 months old) and the size of adolescent/adult spine at the end of growth (animals aged 24 months). However, there are two specific characteristics of the porcine VBs and IVDs that must be taken into account. (1) These

discs have a nucleus that consists primarily of notochordal cells as opposed to the mixture of notochordal cells and fibrous matrix that is found in immature human discs[53,54]. (2) Yucatan mini-pigs (akin to all vertebrates, excluding humans) have vertebrae with ossified and vascularized epiphyseal plates[54]. Consequently, the porcine disc and the physis do not compete for nutrition by the vertebral endplate pathway, potentially making the porcine intervertebral discs less susceptible to degenerative changes[54]. Despite these limitations, since the vertebral[55] and disc[56] morphology and growth rate approximate juvenile and adolescent humans as closely as any animal model, the Yucatan mini-pig is an optimal choice for modeling the immature human spine and quantifying the impact of growth modulating implants.

Specimens

Twelve seven-month old mini-pigs were instrumented with anterolateral thoracic vertebral screws in four consecutive thoracic vertebrae. In six of the animals screws were connected by a polyethylene tether across three adjacent motion segments, while six animals received sham only surgeries (Fig. 5). Animal Care and Use Committee approved study were approved prior to study begin. Sample size was based on a power analysis of previous data on this model for deformity creation (power = 0.8). Instrumentation sites were prepared over four vertebral levels from T8-T11. At each vertebral body, the overlying pleura were incised and the segmental vessel cauterized. Each segment was then instrumented anterolaterally (on the right side) with one specially designed vertebral staple and screw (with a maximum outer diameter of 9 7.5mm and length of 35mm; DePuy Spine Inc., Raynham, MA). During implantation, neither the discs nor growth plates were disturbed. In six animals, the vertebral body screws were aligned and an ultra-high molecular weight polyethylene (UHMWPE) ribbon tether (cross section, 1.5 x 7.5mm) was placed and fastened to the screws, connecting the four vertebrae (Tether Group). All tethers

were tensioned so that the slack was taken out of the system, yet spinal alignment was not affected. No tether was placed in the screws of the remaining six animals (sham surgery, Control Group). Routine closure of the thoracotomy was then performed over a chest tube. Following each surgery, post-operative radiographs were obtained.

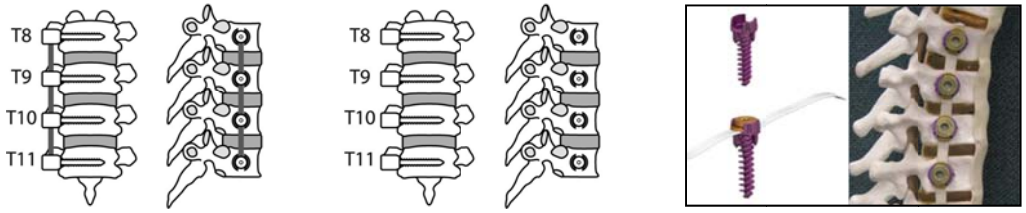

Group 1- Tethered **Group 2- Sham** **Tethering System**

Figure 5: Experimental groups; Right image: Tether and tether placement in a saw bone model

Radiographic Analysis and 2D Computed Tomography Evaluation

All animals survived for six months following tether placement and monthly dorso-ventral and lateral radiographs of the spine were obtained. After six months, all thoracic spines were harvested en bloc to include vertebral levels T7-T12. Biplanar (Dorsoventral, lateral) 2D digital plain radiographic imaging was performed on all spines in each group following harvest. Degree of scoliosis and sagittal alignment (Cobb angle measured from the four instrumented levels), as well as the individual vertebral body and disc space wedging were performed for each thoracic segment and the disc space heights were measured off the DV and lateral x-rays (Fig. 6 A and B). Immediately following harvest, computed tomography (CT) scans were obtained of the fresh spines with the instrumentation in position. Vertebral body and disc space heights in the coronal (right versus left) and sagittal (anterior versus posterior) planes were measured for the four instrumented vertebrae (T8, 9, 10 and 11) and four adjacent vertebrae (T6, T7 and T12, T13), as well as the three intervening discs (T8-9, T9-10, T10-11) and four adjacent discs (T6-7, T7-8 and T11-12, T12-13). Vertebral rotation was also measured using CT images in the axial plane.

Rotation was measured as the angle formed between a vertical line bisecting the vertebral body / spinous process and the true horizontal (Fig. 6C). Rotation of the L1 vertebral body was used as a baseline, with rotation of the other vertebral bodies reported as relative to L1.

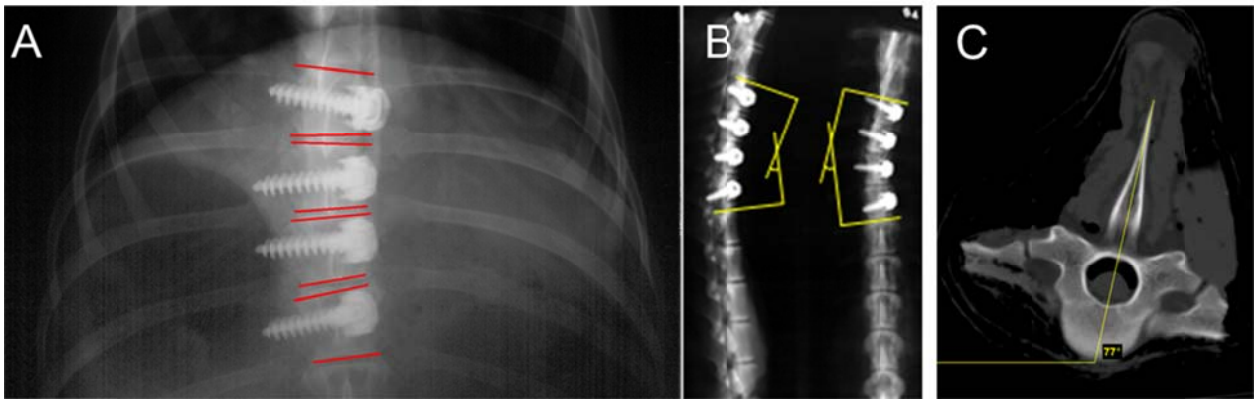

Figure 6: Vertebral height measurements (A); Scoliosis and kyphosis Cobb angle (B); Vertebral rotation measured using 2D CT imaged in the axial plane (C).

All measurements were performed using Amicas LightView^{TM} Vision Series PACS (v. 5.0, Amicas, Brighton, MA, USA). Measurements were done from two separate researchers on two separate occasions, to measure intra- and inter-observer reliability.

MIMICS 3D Reconstructions

Surface reconstructions of individual vertebra and disc space from CT scans, discs from MRI, physis and endplates from μCT were created using Mimics 14 (Innovation Suite, Materalize, Leuven, Belgium).

Surface reconstructions of individual vertebrae from CT scans (Fig. 7), discs from MRI (Fig. 8), physis and endplates from μCT (Fig. 9) were created using Mimics. For vertebra reconstruction, thresholding was used to select all bone, and individual vertebrae were separated manually. Artifacts created by instrumentation were corrected as necessary. The disc spaces were created later in a separate MATLAB application from the inferior surface of the endplate of the top vertebra and the superior surface of the endplate of the lower vertebra. For the disc reconstruction from MRI, simple thresholding was used to select the discs. Endplates and adjacent vertebral bodies were reconstructed from μCT scans in the same way as the vertebrae were reconstructed from the CT scans. Once complete, STL (stereolithography CAD) models of each vertebra, disc, and endplate were exported for analysis.

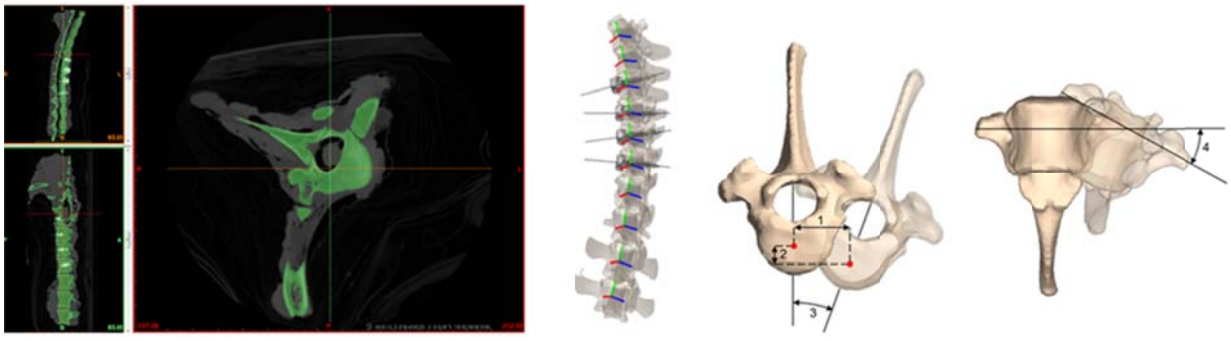

Figure 7: CT scans of the entire spine, 3D reconstruction with spinal orientation and single vertebra analysis (from left).

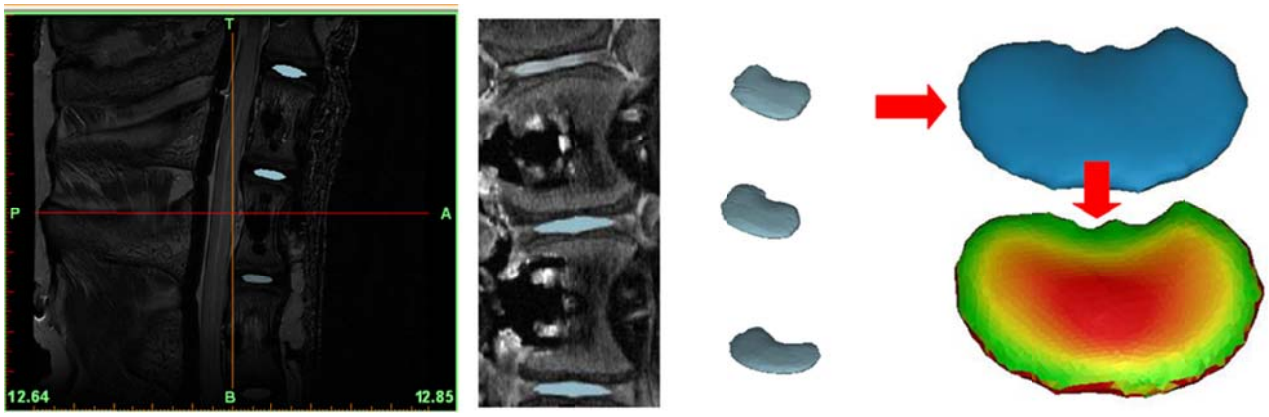

Figure 8: MRI scans of the entire spine and 3D disc reconstruction.

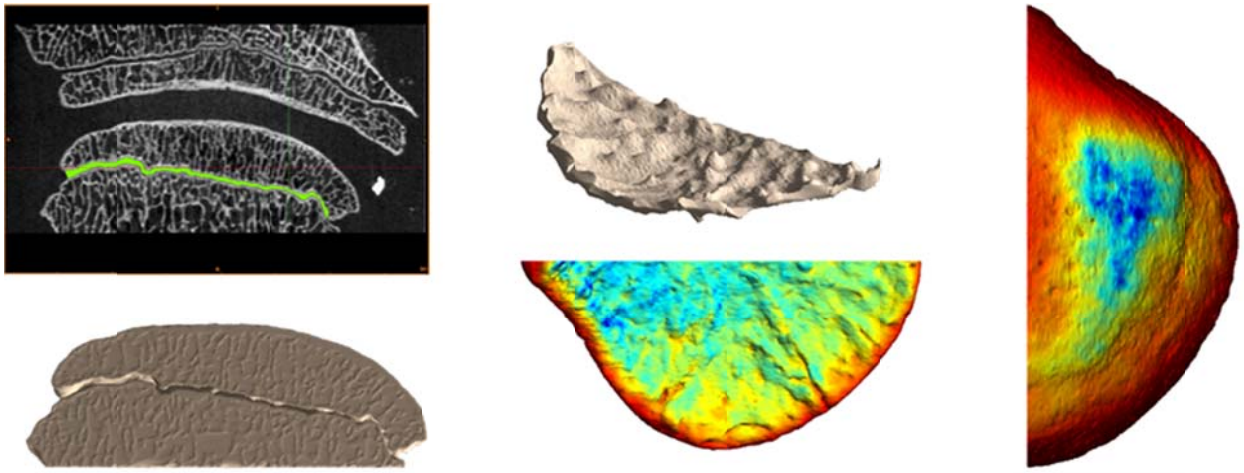

Figure 9: Micro CT reconstruction of the growth plate (physis) and endplates.

Morphological Analysis

The 3D reconstructions of vertebra, disc space, disc, growth plates and endplates were exported from MIMICS as STL files and loaded to a custom MATLAB application. Principal axes were calculated for each vertebra using spinal canal orientation and the best plane of symmetry. Points of interest including vertebral body center, spinal canal center, and endplate centers were calculated for each vertebra to facilitate later analyses. Superior and inferior endplates surfaces of each vertebra were identified. The orientation of each endplate was characterized using least-squares planar regression and inertial eigenvector analysis of surface points. To calculate

vertebral body wedging, the angles between the superior and inferior endplate orientation vectors were calculated (Fig. 10). Disc space wedging was calculated in the same way using endplates of adjacent vertebrae (Fig. 11). Orientation vectors will be projected into different planes (vertebral sagittal, vertebral coronal, instrument normal plane) to calculate wedging in different directions.

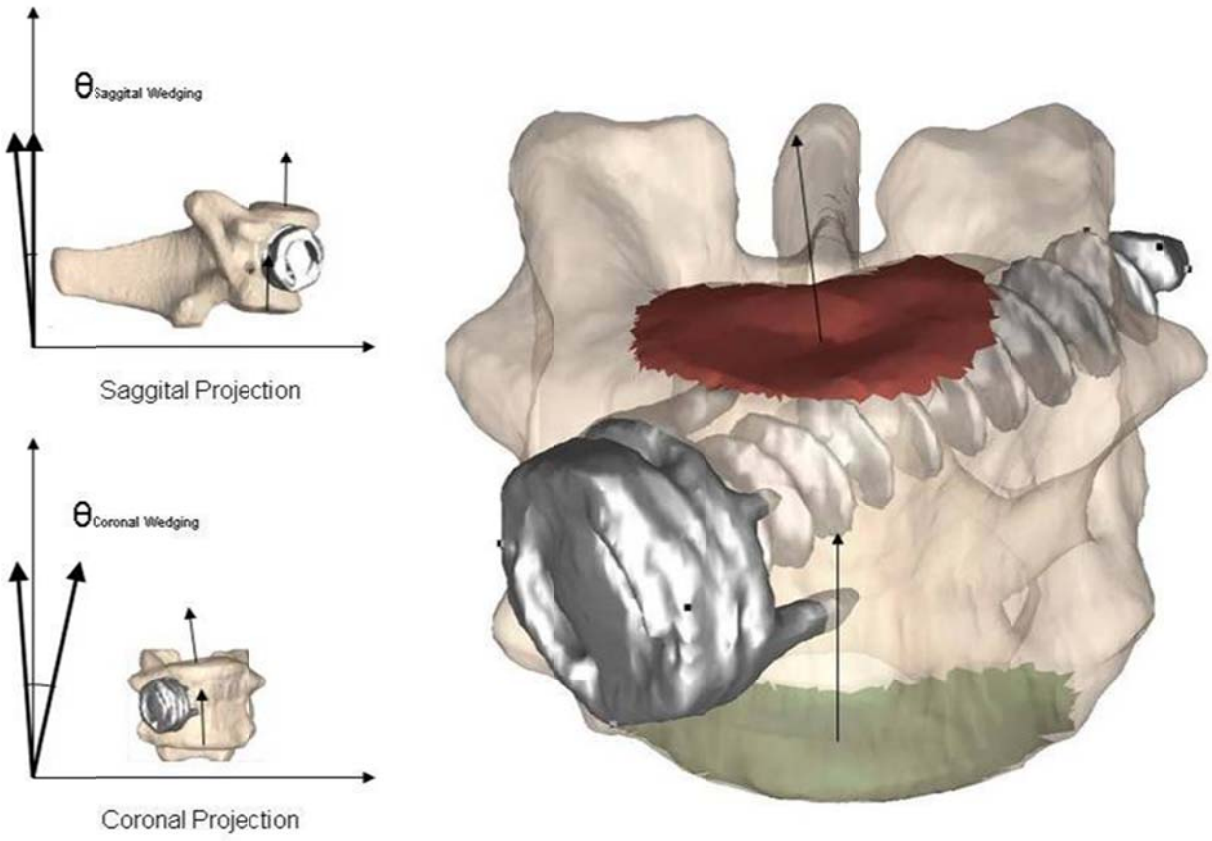

Figure 10: Vertebra orientation, wedging and eigenvector identification.

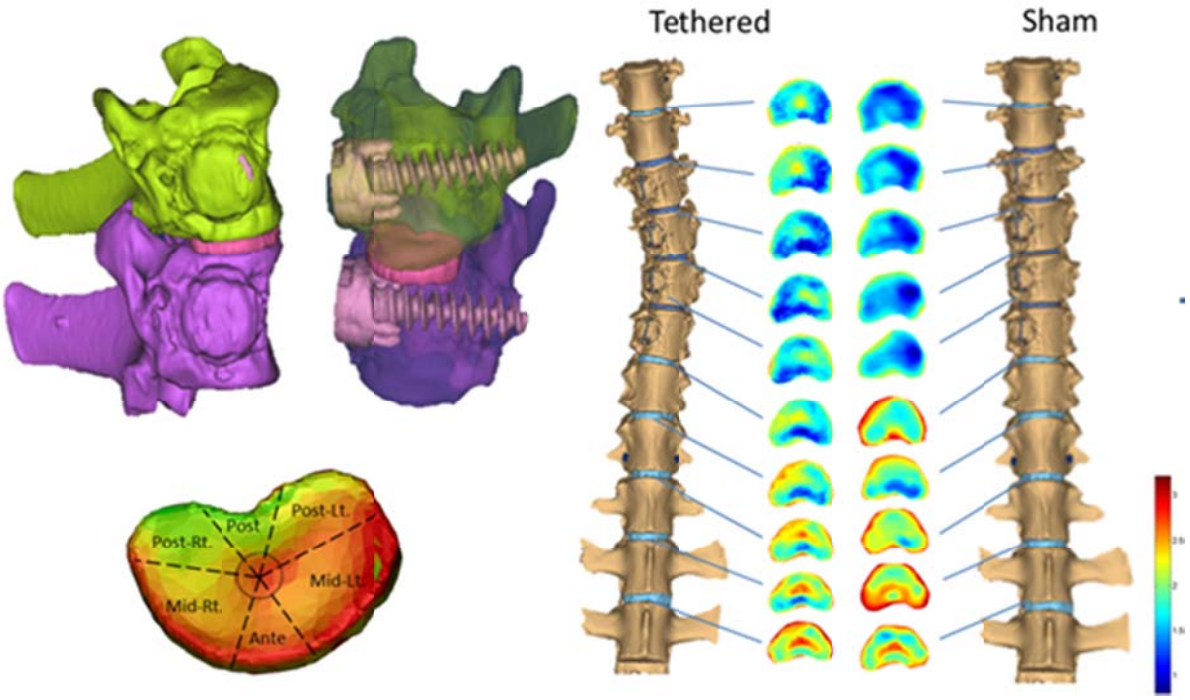

Figure 11: Disc space from CT and discs from MRI reconstruction and analysis. Color map represents the different heights in the discs with red being larger than blue.

Principal axes for each whole spine were calculated using vertebral body centers of pre-determined cranial and caudal neutral vertebrae. Once each spine has been oriented, whole spine deformation metrics was computed. As described in Negrini et. al,[44] vertebral body centers were projected onto the transverse plane and connected with a spline (Fig. 12). The area, direction, and thickness (phase) of the resulting polygon was computed. Also, a Da Vinci diagram was created for each spine, as described in Sangole et. al.[58] The Da Vinci diagram entails dividing the spine into proximal-thoracic, thoracic, and lumbar regions, calculating the plane of maximum Cobb angle for each region. The maximum Cobb angle and the angle of the plane are plotted as vectors on a polar plot.

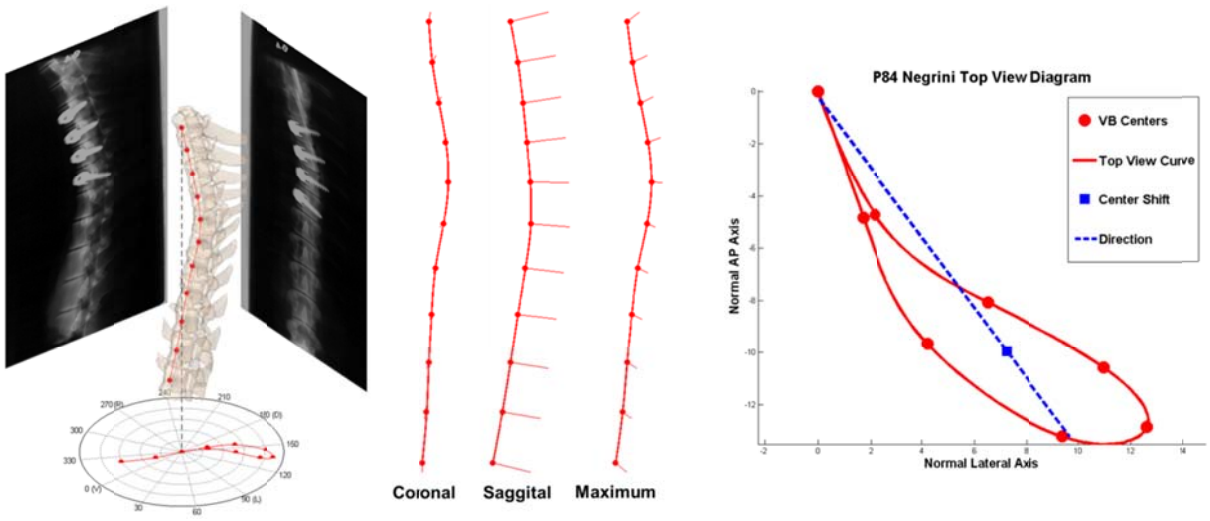

Figure 12: Vertebra body centers (centroids) used to define global spinal parameters.

Discs spaces were analyzed using planar regressions and inertial eigenvectors of the superior and inferior surfaces, just as with the vertebral bodies and disc spaces. Disc height color maps and volumes were also calculated. The disc was divided in different regions to facilitate better comparison between the effected disc sections and heights were averaged within each sector (Fig. 13). The center area was defined by shrinking the edges of the disc so that the area of the center region was approximately 1/5 of the total area of the disc cross section.

A comparison between the disc space and the disc itself was performed. MicroCT endplate reconstructions were analyzed at specific regions of interest for bone density and trabecular structure. Bone density was computed by averaging pixel from unprocessed μCT data. Surface area to volume ratios of trabecular bone surface reconstructions were calculated and used as a measure of trabecular structure. Endplate volume and thickness distribution was also calculated. Physes volume and thickness distributions were calculated using surface-to-surface distance maps of endplate and vertebral body surfaces calculated from μCT scans. Because of the typical undulating shape of physes, they were analyzed using sector analysis instead of planar analysis;

each growth plate was divided into sectors, and the average thickness of each sector will be reported. All calculations were performed using MATLAB.

Results for each deformation metric were compared across experimental groups. In particularly, vertebra and disc space wedging in coronal, sagittal and maximal direction were determined and compared between tethered and sham group.

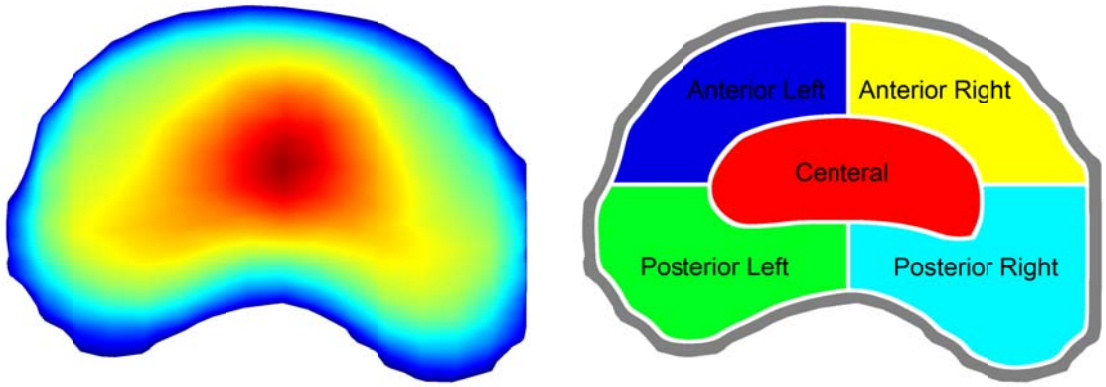

Figure 13: Continuous color map of the disc thickness (left) and disc sectors selected for statistical analysis (right).

Statistical Analysis

Commercial software (SPSS Inc., Chicago, IL) was used to evaluate the differences between the two groups (tethered and sham) on all of the parameters described. Continuous data was checked for normality and homogeneity of variances prior to utilization of parametric tests. Should either of these assumptions be violated, logarithmic transformation of the data or nonparametric alternatives was employed as appropriate. Statistical significance was determined using an alpha level of 0.05.

For the x-ray and 2D measurements, repeated measures analyses of variance (MANOVA) were utilized to compare tethered and sham group. This includes vertebra body and disc space wedging, and disc space heights. Additionally, the inter- and intra-observer agreement regarding the measurements from x-ray and 2D CT was assessed with the use of the intra- and inter-class correlation coefficients to identify the repeatability and reliability of the 2D method. Similarly, all parameter extracted from the 3D reconstructed models were statistically evaluated to determine differences between tethered and sham group using MANOVA and p-value of 0.05. Furthermore, regression analysis using the least square approach was performed to determine the relationship between the different parameter extracted from the different techniques (x-ray vs. 2D CT, x-ray vs. 3D CT, and 2D vs. 3D CT).

RESULTS

Global Deformation

Two-dimensional x-ray ($p=0.01$) and 3D CT ($p=0.045$) resulted in significantly increased Cobb angle in the coronal plane in the tethered group, while the sagittal alignment was maintained with no difference between the groups (Fig. 14 left). There was no significant difference between the x-ray and 3D CT results. The maximum Cobb calculated from the 3D CT was larger than the individual coronal and sagittal plane angles (17.4±4.8° and 27.4±5.4° for the sham and tethered group, respectively) and was on average 32° off of the local vertebrae coronal lateral axis (roughly in the middle between the DV and lateral plane views). X-ray and CT Cobb angles in both planes showed excellent correlation (Fig. 14 right, $R^2=0.93/0.66$ for DV/Sag Cobb respectively)

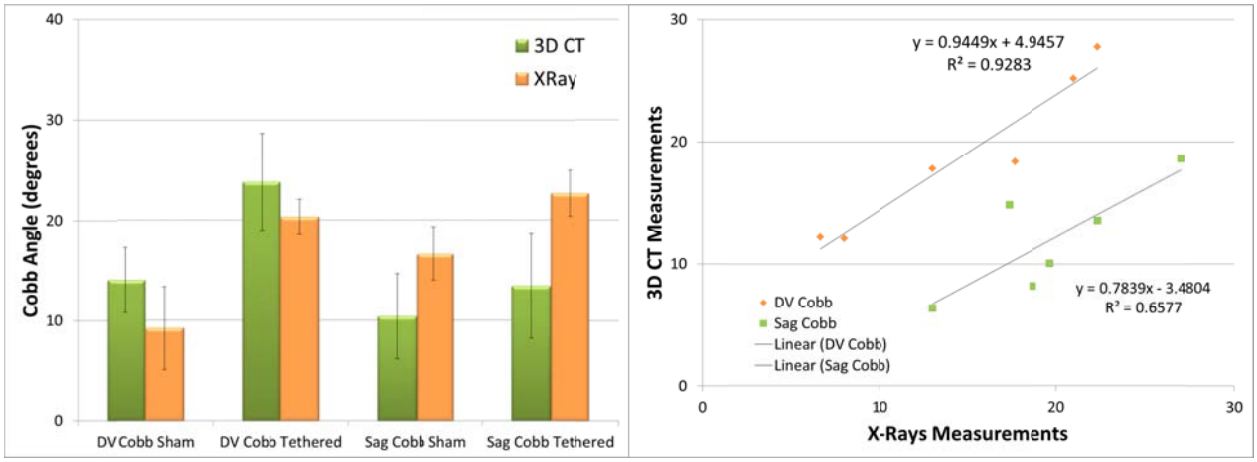

Figure 14: Coronal (DV) and lateral (Sag) Cobb angle determined by x-ray and 3D CT (left); Correlation between X-Ray and 3D CT for DV and Sag Cobb.

For the axial rotation, the adjacent (T6, T7, T12, T13) and the instrumented (T8, T9, T10 and T11) individual vertebrae results were averaged and sham vs. tethered axial rotations were compared (Fig. 15). All rotations are calculated with respect to L1. There was no significant difference between the 2D and 3D CT results (correlation R^2 of 0.87, 0.65 and 0.55 for adjacent levels in sham and tethered spines and instrumented levels in sham spine, respectively); however, the instrumented vertebrae in the tethered group showed opposite trends for both methods with a negative weak correlation (R^2=0.15).

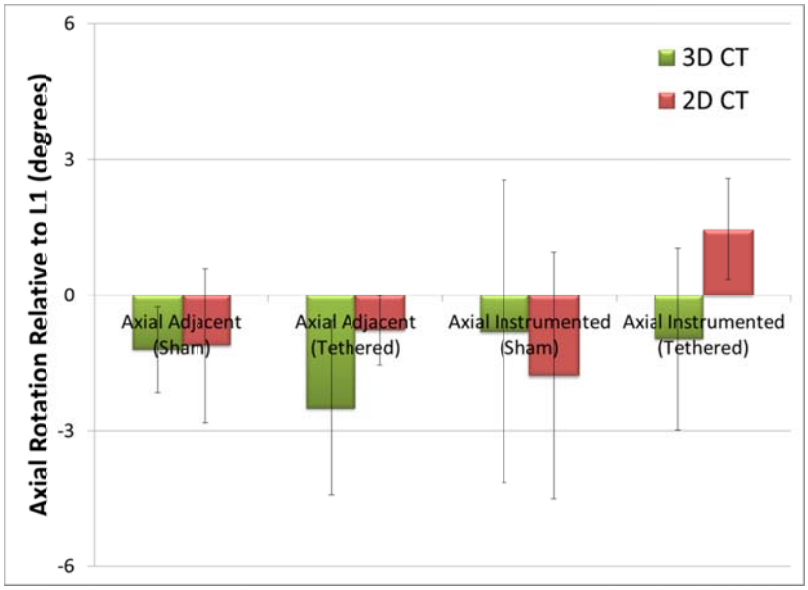

Figure 15: Averaged axial rotation of adjacent and instrumented vertebrae for 2D and 3D CT

Individual Vertebral Body (VB) and Intervertebral Disc (IVD) Results

The coronal plane vertebral body (VB) wedging measured with x-ray resulted in significant higher wedging for the instrumented levels in the tethered group when compared to the same levels in the sham group ($p=0.029$) and approached significance for the adjacent levels ($p=0.07$). However, no significant difference between the same parameters was found when measurements were performed based on the 2D CT scans and 3D CT reconstructions. For the measurements of VB wedging, the lines drawn by the user at a regular x-ray result in greater variation and inconclusive results. CT measurements are recommended when evaluating VB wedging to capture the subtle differences in the angles.

No significant difference between sham and tethered group was found in the adjacent to the instrumentation IVDs with either of the measurement techniques. Disc wedging in the instrumented levels of the tethered spines was significantly smaller than in the sham group ($p<0.02$) with any of the techniques (x-ray, 2D CT and 3D CT). Even though overall disc spaces are very small, trends in the wedging are better captured with the 2D and 3D techniques than in

the VB. There is good correlation between each of the techniques. Disc space height was significantly lower on the right side of tethered group when compared to the sham group, again measured with either technique.

Disc analysis from MRI

There was significant difference between disc heights in the sham group (1.87±0.07mm) when compared to the tethered group (1.65±0.1mm) with the height in the tethered group being lower (Fig. 16, left). In particularly, the anterior right and left sectors were significantly reduced in the tethered group when compared to sham (Fig. 16, right). Interestingly, the disc height was larger anteriorly and narrower posteriorly in the sham group, while the tethered group showed no difference between anterior and posterior region. The center region was nearly identical in the sham and tethered group. The different sectors are defined in Fig. 13. Also, the disc volume was reduced in the tethered group, but not significantly so (174±23mm^3 and 144±11mm^3 for the sham and tethered group, respectively) (Fig. 16, left).

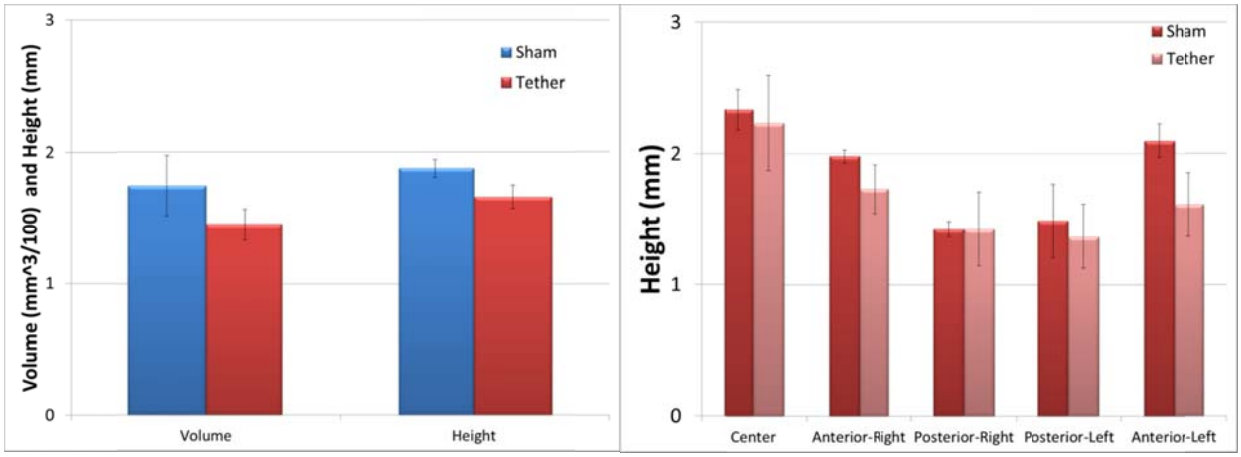

Figure 16: Average disc volume and disc height (left); Disc height in the different identified sectors (right).

Instrumentation

The 3D view of the system allowed for the analysis of the screw placement, which is not possible with either of the 2D methods. We found no significant difference between the tether and sham group screw positioning in terms of angle and offset, assuring consistence and accuracy in the screw placement. This analysis also allowed for evaluating of the wedging parallel and perpendicular to the screw long-axis. Tethered group wedging parallel to the implanted screw resulted in significantly lower disc wedging when compared to the sham group.

Intra- and Inter-Observer Correlation

The reproducibility of each method was tested with the inter- and intra-class correlation (ICC). Two observers performed all measurements at two different occasions, allowing for the identification of the inter- and intra-observer variation. The coronal and sagittal plane Cobb angle measured on the plane x-rays resulted in very high ICC (>0.97). However, ICC was very low for the vertebral body (0.093) and disc wedging (0.048), showing inconsistent results when evaluating those parameters on plane x-rays. 2D CT evaluation resulted in better reproducibility (ICC=0.5 for the VB and 0.4 for IVD). The disc height results based on the x-rays resulted in inconsistent ICC ranging from 0.1 to 0.9. 2D CT measurements were more consistent (ICC=0.4-0.8).

DISCUSSION

The present study assessed the creation of 3D deformity created from a novel fusionless implant. We found greater Cobb angle in the tethered (treated) group when compared to a sham (control) group. The instrument created a complex 3D deformity requiring 3D analysis for complete understanding.

X-ray Cobb angle results correlated very well with 3D measurements. Inter- and intra- class correlation was also very high for the Cobb measurements, indicating good reproducibility of the results. X-rays and 3D CT reconstructions are both very well suited for the analysis of global spinal deformity such as the Cobb angle. 3D reconstructions add additional planes to view the results, such as the identification of the plane of maximal deformation. This evaluation is not possible by a 2D means and adds valuable information to be considered when reviewing 3D deformity.

Axial rotation determined by 2D and 3D CT showed correlation for most of the levels, however, within the tethered group the instrumented levels were negatively correlated between both measurement techniques. This is related to the fact that during the 2D CT measurements the user has to select a plane to perform those measurements. The axial cuts within the 2D CT are based on the global CT coordinate system. A spine that is deformed heavily has its vertebra local coordinate system rotated away from the global CT machine coordinate system, resulting in a greater error within the measurements associated with the 2D technique. The 3D reconstruction allows viewing the spine in the 3D space and creating true local coordinate axes for the calculations.

For the measurements of VB wedging, the lines drawn by the user at a regular x-ray result in greater variation and inconclusive results. CT measurements are recommended when evaluating VB wedging. For the intervertebral disc analysis, all techniques resulted in similar trends with a good correlation between each of the techniques.

New evaluation values were possible when extending the analysis into the 3D space. The 3D view of the system allowed for analysis of the screw placement, which is not possible with either of the 2D methods. This allowed for the evaluation of the accuracy of the screw positioning and

orientation for each of the groups. It also makes it possible to view disc and vertebra wedging among other variables in the plane parallel to the axis of the screw and find changes that may otherwise remain undiscovered.

In summary, the results of this study confirm that 3D analysis using CT, MRI and μCT is reproducible and reliable to determine changes in complex 3D deformities. The correlation between 2D and 3D measurement methods is good for the most parameters. Care is to be taken when created deformity is very large and deviation between local and global coordinate system increases. In such cases, 2D views don't allow for accurate capture of the 3D characteristics and lead to larger errors. However, the sequential measurement of deformity parameters in the course of a study is required because of its cost effectiveness. The accurate measurement extracted from 3D reconstructions can complement the analysis and add additional information to improve the understanding of a complex 3D deformity. Zonal analysis of disc from MRI and disc space from CT also proved to be very useful and revealed a trend for a region-dependent loss of disc height in the tethered group.

REFERENCES

1. Andersson GBJ, Bouchard J, Bozic KJ, et al. The Burden of Musculoskeletal Diseases in the United States ed. Rosemont, IL American Academy of Orthopaedic Surgeons, 2008.
2. Newton PO. Adolescent Idiopathic Scoliosis. 1st ed. Rosemont: American Academy of Orthopaedic Surgeons (AAOS) 2004.
3. Hoh DJ, Elder JB, Wang MY. Principles of growth modulation in the treatment of scoliotic deformities. Neurosurgery 2008;63:211-21.
4. Reamy BV, Slakey JB. Adolescent idiopathic scoliosis: review and current concepts. Am Fam Physician 2001;64:111-6.
5. Nilsonne U, Lundgren KD. Long-term prognosis in idiopathic scoliosis. Acta Orthop Scand 1968;39:456-65.
6. Abe Y, Akeda K, An HS, et al. Proinflammatory cytokines stimulate the expression of nerve growth factor by human intervertebral disc cells. Spine 2007;32:635-42.
7. Wynne-Davies R. Familial (idiopathic) scoliosis. A family survey. J Bone Joint Surg Br 1968;50:24-30.
8. Robin GC, Cohen T. Familial scoliosis. A clinical report. J Bone Joint Surg Br 1975;57:146-8.

9. Dickson RA, Lawton JO, Archer IA, et al. The pathogenesis of idiopathic scoliosis. Biplanar spinal asymmetry. J Bone Joint Surg Br 1984;66:8-15.
10. Jarvis JG, Ashman RB, Johnston CE, et al. The posterior tether in scoliosis. Clin Orthop Relat Res 1988;227:126-34.
11. Piggott H. Growth modification in the treatment of scoliosis. Orthopedics 1987;10:945-52.
12. Smith RM, Dickson RA. Experimental structural scoliosis. J Bone Joint Surg Br 1987;69:576-81.
13. Lowe TG, Edgar M, Margulies JY, et al. Etiology of idiopathic scoliosis: current trends in research. J Bone Joint Surg Am 2000;82-A:1157-68.
14. Miller NH. Genetics of familial idiopathic scoliosis. Clin Orthop Relat Res 2002:60-4.
15. Miller NH. Genetics of familial idiopathic scoliosis. Clin Orthop Relat Res 2007;462:6-10.
16. Chan V, Fong GC, Luk KD, et al. A genetic locus for adolescent idiopathic scoliosis linked to chromosome 19p13.3. Am J Hum Genet 2002;71:401-6.
17. Justice CM, Miller NH, Marosy B, et al. Familial idiopathic scoliosis: evidence of an X-linked susceptibility locus. Spine (Phila Pa 1976) 2003;28:589-94.
18. Wise CA, Barnes R, Gillum J, et al. Localization of susceptibility to familial idiopathic scoliosis. Spine (Phila Pa 1976) 2000;25:2372-80.
19. Alden KJ, Marosy B, Nzegwu N, et al. Idiopathic scoliosis: identification of candidate regions on chromosome 19p13. Spine (Phila Pa 1976) 2006;31:1815-9.
20. Miller NH, Justice CM, Marosy B, et al. Identification of candidate regions for familial idiopathic scoliosis. Spine (Phila Pa 1976) 2005;30:1181-7.
21. Guo X, Chau WW, Chan YL, et al. Relative anterior spinal overgrowth in adolescent idiopathic scoliosis. Results of disproportionate endochondral-membranous bone growth. J Bone Joint Surg Br 2003;85:1026-31.
22. Murray DW, Bulstrode CJ. The development of adolescent idiopathic scoliosis. Eur Spine J 1996;5:251-7.
23. Stokes IA, Spence H, Aronsson DD, et al. Mechanical modulation of vertebral body growth. Implications for scoliosis progression. Spine 1996;21:1162-7.
24. Newton PO, Upasani VV, Farnsworth CL, et al. Spinal growth modulation with use of a tether in an immature porcine model. J Bone Joint Surg Am 2008;90:2695-706.
25. Nachlas IW, Borden JN. The cure of experimental scoliosis by directed growth control. J Bone Joint Surg Am 1951;33:24-34.
26. Mente PL, Stokes IA, Spence H, et al. Progression of vertebral wedging in an asymmetrically loaded rat tail model. Spine (Phila Pa 1976) 1997;22:1292-6.
27. Mente PL, Aronsson DD, Stokes IA, et al. Mechanical modulation of growth for the correction of vertebral wedge deformities. J Orthop Res 1999;17:518-24.
28. Stokes IA, Aronsson DD, Spence H, et al. Mechanical modulation of intervertebral disc thickness in growing rat tails. J Spinal Disord 1998;11:261-5.
29. Newton PO, Farnsworth CL, Faro FD, et al. Spinal growth modulation with an anterolateral flexible tether in an immature bovine model: disc health and motion preservation. Spine (Phila Pa 1976) 2008;33:724-33.
30. Newton PO, Faro FD, Farnsworth CL, et al. Multilevel spinal growth modulation with an anterolateral flexible tether in an immature bovine model. Spine (Phila Pa 1976) 2005;30:2608-13.

31. Newton PO, Fricka KB, Lee SS, et al. Asymmetrical flexible tethering of spine growth in an immature bovine model. Spine (Phila Pa 1976) 2002;27:689-93.
32. Newton PO, Farnsworth CL, Upasani VV, et al. Effects of Intraoperative Tensioning of an Anterolateral Spinal Tether on Spinal Growth Modulation in a Porcine Model. Spine (Phila Pa 1976) 2010.
33. Braun JT, Akyuz E, Ogilvie JW, et al. The efficacy and integrity of shape memory alloy staples and bone anchors with ligament tethers in the fusionless treatment of experimental scoliosis. J Bone Joint Surg Am 2005;87:2038-51.
34. Braun JT, Ogilvie JW, Akyuz E, et al. Fusionless scoliosis correction using a shape memory alloy staple in the anterior thoracic spine of the immature goat. Spine (Phila Pa 1976) 2004;29:1980-9.
35. Braun JT, Hoffman M, Akyuz E, et al. Mechanical modulation of vertebral growth in the fusionless treatment of progressive scoliosis in an experimental model. Spine (Phila Pa 1976) 2006;31:1314-20.
36. Braun JT, Akyuz E, Udall H, et al. Three-dimensional analysis of 2 fusionless scoliosis treatments: a flexible ligament tether versus a rigid-shape memory alloy staple. Spine 2006;31:262-8.
37. Braun JT, Hines JL, Akyuz E, et al. Relative versus absolute modulation of growth in the fusionless treatment of experimental scoliosis. Spine (Phila Pa 1976) 2006;31:1776-82.
38. Braun JT, Ogilvie JW, Akyuz E, et al. Experimental scoliosis in an immature goat model: a method that creates idiopathic-type deformity with minimal violation of the spinal elements along the curve. Spine (Phila Pa 1976) 2003;28:2198-203.
39. Betz RR, D'Andrea LP, Mulcahey MJ, et al. Vertebral body stapling procedure for the treatment of scoliosis in the growing child. Clin Orthop Relat Res 2005:55-60.
40. Betz RR, Kim J, D'Andrea LP, et al. An innovative technique of vertebral body stapling for the treatment of patients with adolescent idiopathic scoliosis: a feasibility, safety, and utility study. Spine 2003;28:S255-65.
41. Guille JT, D'Andrea LP, Betz RR. Fusionless treatment of scoliosis. Orthop Clin North Am 2007;38:541-5, vii.
42. Stokes IA, McBride CA, Aronsson DD. Intervertebral disc changes in an animal model representing altered mechanics in scoliosis. Stud Health Technol Inform 2008;140:273-7.
43. Mok SS, Masuda K, Hauselmann HJ, et al. Aggrecan synthesized by mature bovine chondrocytes suspended in alginate. Identification of two distinct metabolic matrix pools. J Biol Chem 1994;269:33021-7.
44. Lai A, Chow DH, Siu SW, et al. Effects of static compression with different loading magnitudes and durations on the intervertebral disc: an in vivo rat-tail study. Spine (Phila Pa 1976) 2008;33:2721-7.
45. Upasani VV, Farnsworth CL, Chambers RC, et al. Intervertebral Disc Health Preservation after Six Months of Spinal Growth Modulation: Expanding the Treatment Options for Fusionless Spinal Deformity Correction. J Bone Joint Surg Am 2010.
46. Hunt KJ, Braun JT, Christensen BA. The effect of two clinically relevant fusionless scoliosis implant strategies on the health of the intervertebral disc: analysis in an immature goat model. Spine (Phila Pa 1976) 2010;35:371-7.
47. Blount WP. A mature look at epiphyseal stapling. Clin Orthop Relat Res 1971;77:158-63.

48. Blount WP, Clarke GR. The classic. Control of bone growth by epiphyseal stapling. A preliminary report. Journal of Bone and Joint Surgery, July, 1949. Clin Orthop Relat Res 1971;77:4-17.
49. Smith AD, Von Lackum WH, Wylie R. An operation for stapling vertebral bodies in congenital scoliosis. J Bone Joint Surg Am 1954;36:342-8.
50. Roaf R. The Treatment of Progressive Scoliosis by Unilateral Growth-Arrest. J Bone Joint Surg Br 1963;45:637-51.
51. Cho TJ, Choi IH, Chung CY, et al. Hemiepiphyseal stapling for angular deformity correction around the knee joint in children with multiple epiphyseal dysplasia. J Pediatr Orthop 2009;29:52-6.
52. Staheli LT. Normative data in pediatric orthopedics. J Pediatr Orthop 1996;16:561-2.
53. Butler WF. Comparative anatomy and development of the mammalian disced. Boca Raton, FL: CRC, 1988.
54. Alini M, Eisenstein SM, Ito K, et al. Are animal models useful for studying human disc disorders/degeneration? Eur Spine J 2008;17:2-19.
55. McLain RF, Yerby SA, Moseley TA. Comparative morphometry of L4 vertebrae: comparison of large animal models for the human lumbar spine. Spine (Phila Pa 1976) 2002;27:E200-6.
56. Wang JL, Tsai YC, Wang YH. The leakage pathway and effect of needle gauge on degree of disc injury post anular puncture: a comparative study using aged human and adolescent porcine discs. Spine (Phila Pa 1976) 2007;32:1809-15.
57. Stokes IA, Mente PL, Iatridis JC, et al. Enlargement of growth plate chondrocytes modulated by sustained mechanical loading. J Bone Joint Surg Am 2002;84-A:1842-8.
58. Bylski-Austrow DI, Wall EJ, Glos DL, et al. Spinal hemiepiphysiodesis decreases the size of vertebral growth plate hypertrophic zone and cells. J Bone Joint Surg Am 2009;91:584-93.
59. Jadin KD, Wong BL, Bae WC, et al. Depth-varying density and organization of chondrocytes in immature and mature bovine articular cartilage assessed by 3d imaging and analysis. J Histochem Cytochem 2005;53:1109-19.
60. Hicks DL, Sage AB, Schumacher BL, et al. Stored human septal chondrocyte viability analyzed by confocal microscopy. Arch Otolaryngol Head Neck Surg 2006;132:1137-42.
61. Chao EYS, Inoue N, Elias JJ, et al. Computational biomechanics using image-based models. In Frank J, Brody W, Zerhouni E eds. Handbook of Medical Image Processing San Diego, CA: Academic Press, 2000:29.
62. Sugisaki K, An HS, Espinoza Orias AA, et al. In vivo three-dimensional morphometric analysis of the lumbar pedicle isthmus. Spine (Phila Pa 1976) 2009;34:2599-604.
63. Johannessen W, Auerbach JD, Wheaton AJ, et al. Assessment of human disc degeneration and proteoglycan content using T1rho-weighted magnetic resonance imaging. Spine (Phila Pa 1976) 2006;31:1253-7.
64. Auerbach JD, Johannessen W, Borthakur A, et al. In vivo quantification of human lumbar disc degeneration using T(1rho)-weighted magnetic resonance imaging. Eur Spine J 2006;15 Suppl 3:S338-44.
65. Roberts S, Urban JP, Evans H, et al. Transport properties of the human cartilage endplate in relation to its composition and calcification. Spine 1996;21:415-20.

66. Lu W GG, Butts KR, Pauly J, Hargreaves BA. Distortion-free magnetic resonance imaging near metallic implants. . Proc Radiol Soc NA 94th Scientific Assembly and Annual Meeting. Chicago, IL, 2008:411.
67. McGowan KB, Kurtis MS, Lottman LM, et al. Biochemical quantification of DNA in human articular and septal cartilage using PicoGreen and Hoechst 33258. Osteoarthritis Cartilage 2002;10:580-7.
68. Farndale RW, Buttle DJ, Barrett AJ. Improved quantitation and discrimination of sulphated glycosaminoglycans by use of dimethylmethylene blue. Biochim Biophys Acta 1986;883:173-7.
69. Woessner JF, Jr. The determination of hydroxyproline in tissue and protein samples containing small proportions of this imino acid. Arch Biochem Biophys 1961;93:440-7.
70. Morrison TB, Weis JJ, Wittwer CT. Quantification of low-copy transcripts by continuous SYBR Green I monitoring during amplification. Biotechniques 1998;24:954-8, 60, 62.
71. Masuda K. Biological repair of the degenerated intervertebral disc by the injection of growth factors. Eur Spine J 2008;17 Suppl 4:441-51.
72. Boos N, Weissbach S, Rohrbach H, et al. Classification of age-related changes in lumbar intervertebral discs: 2002 Volvo Award in basic science. Spine 2002;27:2631-44.
73. Glaser DA, Nandipati C, Nunn T, et al. Biomechanics of Two Fusionless Scoliosis Correction Techniques- Rigid Staple vs. Flexible Tether American Academy of Orthopaedic Surgeons. San Diego, CA, 2011.